Statistical Beam-Hardening Correction for Industrial X-ray Computed Tomography

Raphaël THIERRY, Alexander FLISCH, Alice MICELI, Jürgen HOFMANN, Swiss Federal Laboratories for Material Testing and Research (EMPA), Electronic/Metrology Laboratory, Dübendorf, Switzerland

Abstract. We present an industrial X-ray computed tomograph (CT) system used as an integrated dimensional inspection and non-destructive evaluation tool. The Beam-Hardening (BH) effect inherent to the use of polyenergetic X-ray source is one of major source of artefacts for materials of high atomic number. We present a statistical correction method relying on the histogram analysis of a first uncorrected image. At each voxel, the mass attenuation is re-expressed as the weighted sum of the mass attenuation of a given set of reference materials. The method requires a pre-knowledge of the spectrum and detector response or a set of calibration curves. We illustrate the method on a turbine blade in simulation and with experimental data. The results show that the statistical method give undeniable better results and with only few iterations when using accelerations techniques. Moreover the method exhibits its capacity to incorporate *a priori* knowledge, such as constrained density values, non-null support or outer-edge information coming from complementary Non-Destructive modality. Eventually, by reconstructing the density repartition the presented algorithm also display an additional quantitative aspect.

1. Introduction

X-ray CT has become a modern advanced method used in both medical and industrial applications, increasingly moving from 2-D to 3-D modality to allow for significantly improved resolution and gain in acquisition time. Essentially, industrial X-CT applications are characterized by unlimited x-ray dose, higher density engineering materials and/or objects composed of non-overlapping homogeneous geometrical forms.

1.1 Statistical reconstruction in the industrial context

Industrial XCT is frequently employed for non-destructive evaluation of materials in a large set of purposes: flaw detection (pores, bubbles, etc), cracks and delaminations, dimensional characterization for first article inspections [1], and for quantitative evaluation and densitometry [2]. A broad scale of resolution is attainable, from the meter scale (rocket propellers, concrete waste drums of more than one meter in diameter [3], down to nanometric samples of tissues scanned with synchrotron radiation facility [4].
The advent of digital area detectors has brought with it the challenge of achieving image quality comparable to that provided by industrial CT systems equipped with highly collimated and efficient linear detectors arrays [5].
Published results on industrial CT often refer to the Filtered Back Projection (FBP) or the Feldkamp-David-Kreiss (FDK) algorithm for cone beam CT[6]. References to alternative methods, such as statistical algorithm are extremely rare and restrict often to discrete tomography or to the truncated data case ([7], [8]). Statistical algorithms easily take into

account any type of measurement geometry, can incorporate the source/detector response, easily deal with truncated data, object constraints, and any prior knowledge (coupling information from other NDT measuring facilities, material characteristics, etc). They can also handle the nature of the noise distribution, offering lower bias-noise curves [9], and can also model phenomena as scatter and energy dependence, leading to more accurate and artifact-free reconstruction.
Their main drawback is their long computation time. Yet, with the continuing progress of hardware and computing power statistical algorithms progressively find their way into medical X-CT: they outperform analytical methods in metal artifact reduction [10], in limited angle tomography [8], and recently enabled new beam-hardening correction with outstanding results [11]. If the progress in hardware and parallel computing make them now more attractive [12], mathematical solutions were also considered in order to speed up the convergence rate. New Ordered-Subset (OS) scheme now enable an acceleration of the convergence without perturbating the monotonicity [13]. Lastly, it has been assessed that initializing the statistical reconstruction with a Radon inversion (FBP or FDK) suppress the intensity transition artifact and consequently have an acceleration factor of an order of magnitude [14]. Finally combining all these acceleration techniques should render the statistical more tractable.

1.2 The beam-hardening effect

Beam hardening is a process whereby the average energy of the x-ray beam increases as the beam propagates through a material since lower energy x-rays are preferentially attenuated. The energy-dependence of the attenuation coefficient leads to a non-Radon model and artefacts will appear in the reconstructed CT-image. The artefacts are generally characterized by an underestimation of the attenuation coefficient, the “cupping” artefact, and/or by streak-artefact, a strong depression that appears between features of contrasted attenuation [15].
There are a variety of schemes for eliminating beam hardening artefacts in FBP images, including pre-filtering, dual-energy imaging and post-processing techniques ([15-17]). Yan *et al* [18] developed an iterative non-statistical method where two categories of materials are assumed. Recently these methods have been extended to three base classifications [19] and to cone-beam geometry [20]. Alternative statistical approach that models the object attenuation as a linear combination of the attenuation properties of two base substances or more have been proposed [10-11]. These algorithms require knowledge of the polyenergetic source spectrum but do not require any segmentation.

The organisation of the paper is as follows. The section II presents the outline the algorithm. In section III we present simulation results of a turbine-blade in fan-beam geometry and we compare the standard FBP with the statistical reconstruction algorithm. Section IV presents the image reconstruction from real data results.

2. Image Reconstruction

2.1 The measurement model

We model the measurements achieved by a polychromatic interrogation beam by independent Poisson random variables :

$$I_i(s) = Poisson\left\{\int I_0(E)\exp\left(-\int_{L_i(s)}\mu(l,E)dl\right)dE + n(s)\right\} \quad (1)$$

where s is a position on the detector array, $I_0(E)$ is the intensity taking into account both the incident ray source spectrum and the detector sensitivity, $L_i(s)$ symbolises the line of the i-th measurement joining the source centre to the point of detection s, $\mu(l,E)$ being the linear attenuation coefficient at a position l at energy E, and $n(s)$ represents a source of perturbation (scatter, statistical noise, etc…).

2.2 The object model

The essential problem in polychromatic X-ray CT image reconstruction is that the linear attenuation coefficient μ is energy-dependent, so that in addition to being ill-posed, the inverse problem of CT reconstruction becomes underdetermined. We suppose here that the object consists of no more than two identified materials such as the following:

$$\mu(v,E) = \mu^{m}_{mat1}(E)\rho_{mat1}(v) + \mu^{m}_{mat2}(E)\rho_{mat2}(v) \quad (2)$$

where ρ denote the unknown density at a given voxel v of the image and μ^m denote the known ([21]) mass attenuation coefficients for a given material. If we are able to determine the fractions $f_1(v)$ and $f_2(v)$, than we can rewrite the expression of μ with the model :

$$\mu(v,E) = \left(\mu^{m}_{mat1}(E)f_1(v) + \mu^{m}_{mat2}(E)f_2(v)\right)\rho(v) \quad (3)$$

where only the density ρ(v) remains unknown. The simpler option to determine fractions f_1 and f_2 is to perform a first reconstruction of μ and then to segment that image into the two materials. To circumvent the problem of segmentation errors another solution is to model the fractions f_1 and f_2 as functions of ρ [11]. We propose a generalized fraction function determined as follow :

An histogram of the CT image is used to determine the distribution percentage of each material. Thereafter a gaussian distribution is used to fit each peak, and we compute the global image threshold using the Otsu's method [22]. With these parameters one can then fully specify the range of each material. The fraction function is a polynomial that represents the mixture of the adjacent materials, the range of the materials may or may not be overlapping (figure 1).

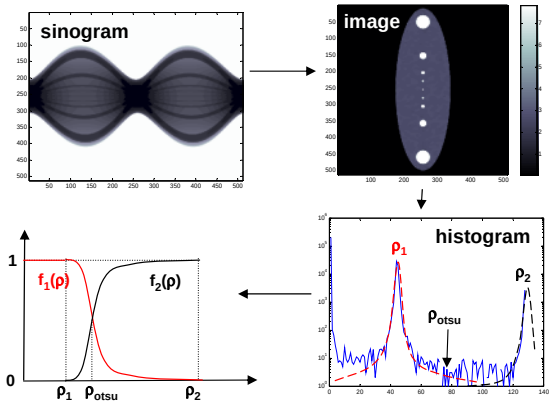

figure 1 : Histogram analysis and determination of polynomial

In this paper, we will illustrate the method with an object composed of a single material; in such case we can model the linear attenuation coefficient as follows:

$$\mu(v,E) = \mu^{m}_{mat}(E)f(v)\rho(v)$$

where the fraction *f* will be chosen given the Gaussian fit, and the Otsu's threshold separating the ground value peak (air and noise) from the peak corresponding to the material.

2.3 The statistical algorithm

We only give the outline in this paper and refer the reader to [11] and [23] for a precise description of the optimization method. We use a maximum *a posteriori* approach ([9], [10]) to estimate the density vector ρ from the measurement model described in equation (1). The penalized log-likelihood for independent Poisson measurements is given by:

$$\begin{aligned}\phi(\rho) &= -L(\rho) + \beta R(\rho) \\ &= \sum_i \{-I_i \, log(E[I_i|\rho]) + E[I_i|\rho]\} + \beta \sum_v \sum_{q \in N(v)} \varphi\left(\frac{\rho_v - \rho_q}{\delta}\right)\end{aligned} \tag{4}$$

where $E[I_i|\rho]$ is the mean of the measured data along path L_i, the hyperparameter β is a positive scalar that realizes the trade-off between the measurement fit and the smoothness and δ is a threshold that handles the dynamic of the image. The function φ is a potential function and N(p) is a neighbourhood clique of voxel v. For our simulation and experimental results, we used for the neighbourhood a clique of the first-order[1] and the convex edge-preserving hyper-surface penalty :

$$\varphi(d\rho) = \sqrt{1 + d\rho^2} \tag{5}$$

The goal of the reconstruction technique becomes to minimize (4) subject to certain object constraints such as non-negativity and with a maximum admitted density, and over a support mask Λ:

$$\begin{cases} \text{if } \rho \in \Lambda, \hat{\rho} = \underset{0 \le \rho \le \rho_{max}}{arg\,min}\ \phi(\rho), \\ \text{elsewhere } \hat{\rho} = 0, \end{cases} \tag{6}$$

An iterative algorithm based on the optimization transfer principle [23] has been employed to achieve the minimization of the constrained non-linear problem (6). The optimization transfer method ensures that the cost function decreases monotonically at each iteration; yet because of the non-convex likelihood term, the algorithm is not guaranteed to converge to the global minimum. The resulting algorithm is a cost function Ψ that is quadratic and separable in ρ, and the iterative scheme uses a Newton scheme:

$$\rho^{n+1} = \rho^n - \frac{\dot{\psi}(\rho^n)}{\ddot{\psi}(\rho^n)} \tag{7}$$

where $\dot{\psi}, \ddot{\psi}$ are respectively the gradient and the Hessian of the cost function.

We use ordered subsets to accelerate the algorithm, and made use of symmetries in the geometry of the measurements in order to speed up the projector/backprojector pair. With two materials, the iteration involves two forward projections and two backprojections, therefore for n iterations, the algorithm is roughly equivalent to 4n runs of FBP. In our application, with a good starting image (generally a FBP reconstruction), and with the help of ordered subsets, a good image quality can be achieved with a decade of iterations.

2.4 Energy Spectrum Calibration

Most often, empirical measurements are utilized in industrial X-CT for post-processing beam-hardening correction. They are based on producing a set of calibration data by

[1] a clique of first order is constituted by the two horizontal and the two vertical neighbours in 2D, plus the two vertical neighbours in 3D.

scanning of regular shapes of the material of interest, e.g. step-wedges or triangular wedges. This approach is time-consuming and sensible to alignment errors during the scanning process. Moreover, the calibration remains valid for a specific material, source setting and additional filtration: any change in these parameters would require a new calibration series. Lastly, in cone-beam geometry, there is substantial error in these measurements due to the significant contributions of object scattering.
The approach reported here consists of a Monte-Carlo simulation-based correction with the simulation tool Geant4 [24]. The simulations are easily calculated within a few hours for an arbitrary combination of source energy/voltage, anode angle, filter, and object material. The errors limiting accuracy of the measurement process are eliminated. Beside the Monte-Carlo approach, we also used the experimental measurements of step-wedges of different materials of interest in order to validate the simulation and the final results (figure 2).

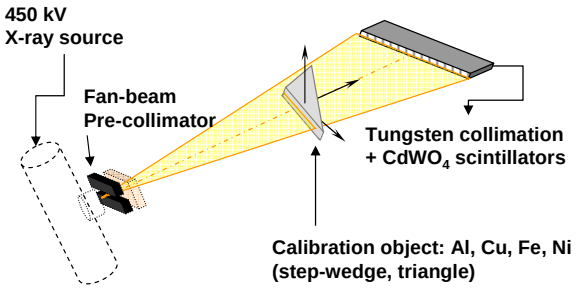

figure 2 : Schematic setup for calibration measurements

On figure 3, we show the experimental attenuation curve (in blue) for the material composing the object under study in this paper. We used this experimental calibration curve for the correction of the beam-hardening in the FBP method. The simulated attenuation (in green) is in good agreement excepted for the longest path ways. The limited dynamic of the detector has indeed not been taken into account in the Monte-Carlo simulation, which explains the discrepancy. The non-linearity of the beam-hardening is illustrated with the plot of the equivalent attenuation of a monochromatic beam at 236 keV, the mean energy of the interrogating beam.

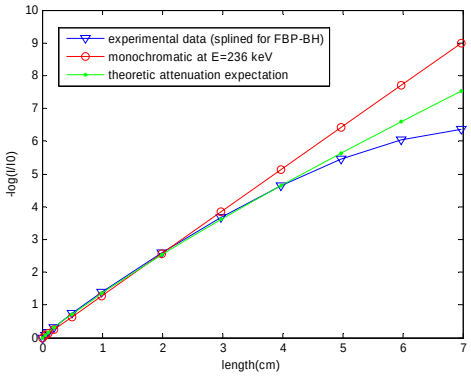

figure 3 : Experimental and simulated Calibration curve

3. Reconstruction Results with Simulated Data

3.1 Acquisition parameters and simulated phantom

We investigated a turbine-blade phantom (figure 4) which has been obtained after an appropriate segmentation of a CT image reconstruction of a real turbine blade. We simulated the same material as the one constituting the real turbine, a Nickel Alloy of

density 8.11 g/cm^3, and we added four drills of respectively 0.6, 0.8, 1.0 and 1.2 mm. Theses gaps where added along the longest path length along the object, which is of 7.6 cm. For a mean energy of 236 keV, this correspond to an attenuation factor of 9.89, and correspond to a dynamic range of 14.3. This is an ideal case and is treated in the paragraph 3.2. To simulate a real detector we reduced the dynamic to 8.9 bit, and to render the problem more challenging we also diminished the number of projections angles : this case will be treated in 3.3.

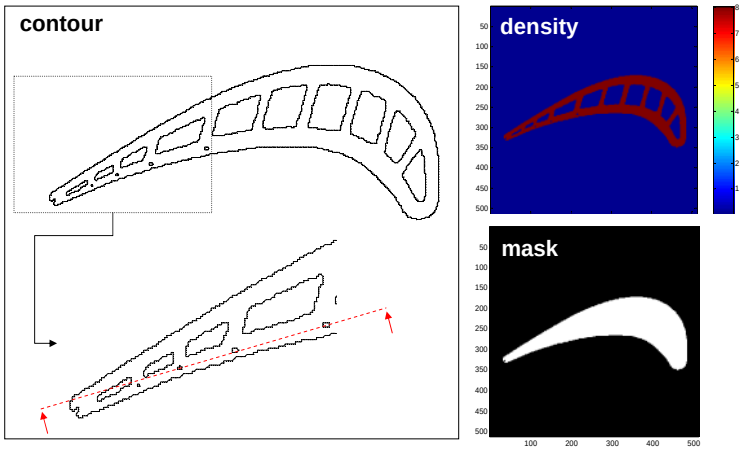

figure 4 : Simulated Turbine-Blade with defects (holes): contour, density and mask. The dotted red line correspond to the profile we used throughout the study

We used the classical "FBP" for the analytical reconstruction method. We used a Hamming window with a cutoff frequency at 0.8. We corrected the BH in the FBP image with the available calibration curve: the "FBP,BHCe" and "FBP,BHC" respectively refer to a correction with the experimental curve and the simulated curve (see figure 3). Finally, the FBP images were rescaled in order to be comparable with the density image reconstructed by the statistical images. We use two versions of the statistical algorithm :

- the first one, referred as "STAT", uses only the constraint over the minimum and maximum value of the density ($0 \le \rho \le \rho_{max} = 8.11\,\mathrm{g/cm^3}$);
- the second one, referred as "STAT,MASK", in addition to the constraint over the minimum and maximum value, reconstruct the density over the mask (all pixels outside the mask are automatically set to zero).

The hyperparameters (β,δ) intervening in the statistical algorithms were both chosen experimentally, and we used 32 subsets to accelerate the convergence.
The image quality is measured with the normalized mean square error (NMSE); for the iterative methods employed, the NMSE is recalculated at each iteration p such as follows :

$$\mathrm{NMSE}(p) = \left(\frac{\sum_i (\rho_j^p - \rho_j^*)^2}{\sum_i (\rho_j^*)^2} \right)^{\frac{1}{2}} \qquad (8)$$

where ρ^* is the density of the exact phantom.

3.2 Results with Ideal measurements

Fig. 5 shows the reconstruction of the phantom with ideal simulated measurements (no noise, unlimited dynamic range). We simulated 512 projections in 2D fan-beam geometry over [0, 2π], with 601 detectors, and the images are 15 cm × 15 cm and 512 × 512 pixels, so a pixel resolution of 0.29 mm. The profile was acquired along a line crossing the hole as described in figure 4. For polychromatic simulation, the FBP results in a slight amount of cupping : this cupping is entirely eliminated in the FBP,BHC and in the statistical versions

as well. The statistical methods exhibit a good capacity to reconstruct smooth and noise-free piecewise regions interrupted with sharp edges. The graph of the residual error shows a clear superiority of STAT,MASK: with 10 iterations STAT,MASK has a NMSE of 0.13, compared to 0.17 for STAT, 0.21 for FBP,BHC and 0.25 for FBP.
In term of image quality, the FBP,BHC and the STAT,MASK are similar, only the analysis of the profile and the NMSE permits to state the superiority of the statistical algorithm. We also observe that the gain in quality is little after 20 iterations and so it constitutes a good compromise between reconstruction time and quality. FBP-like image reconstruction was realized in 10 seconds in a Pentium 4 CPU, 2.8 GHz, whereas the 20 iterations of STAT need 10 minutes.

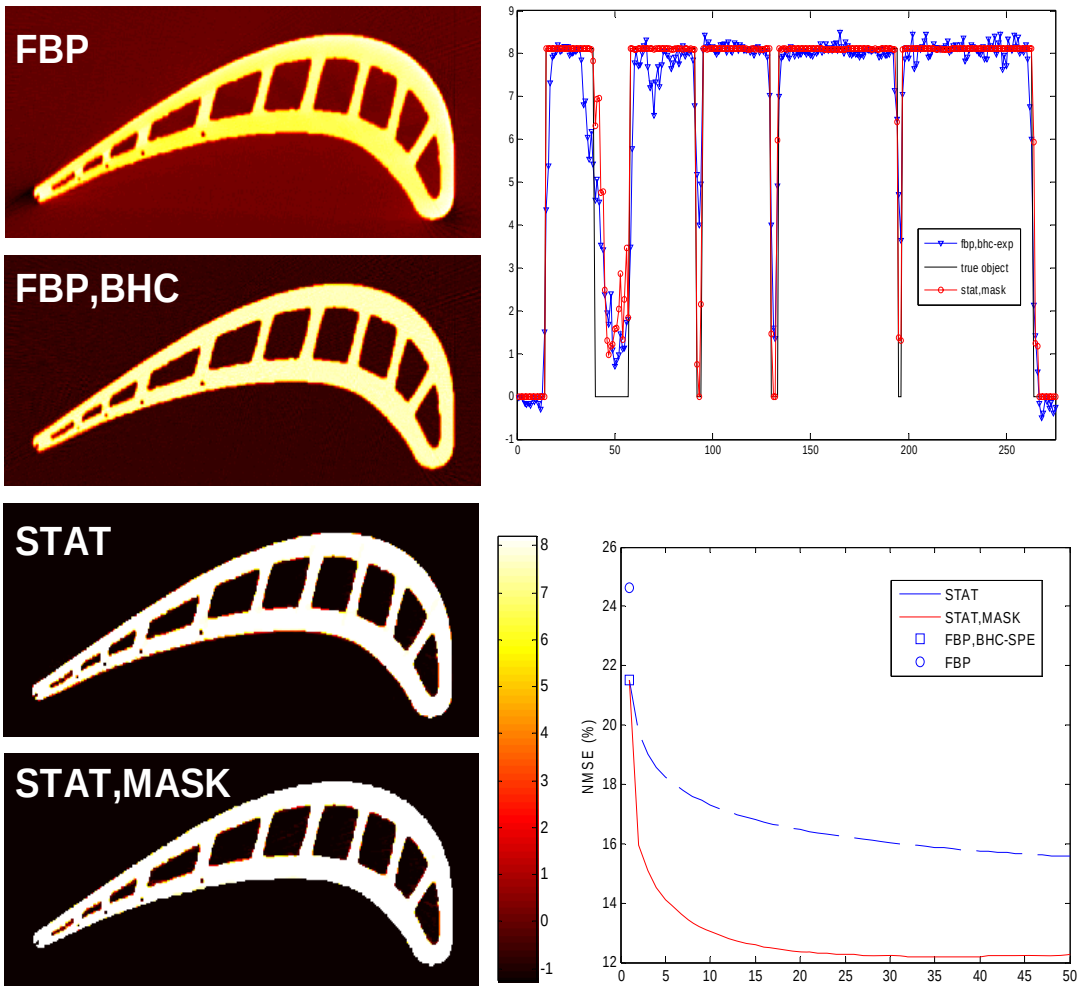

figure 5 : Reconstructed images, profile and NMSE

3.3 Results with reduced projections and limited dynamic range

Fig. 6 shows the reconstruction of the phantom with realistic simulated measurements. To simulate the real detector, we post-processed the simulated attenuation in the sinogram with the experimental calibration curve (figure 3). Conjointly we reduced the projections to 256. The rest of the parameters were kept as in paragraph 3.2 The FBP results now in a substantial amount of cupping in the longest pathway, and we observe additional streaks due to the limited data. The cupping is only partly eliminated in the FBP,BHC, because it relies on the simulated attenuation curve. Naturally the correction improves when using the experimental calibration curve as in FBP,BHCe. Yet a clear crack-shaped artefact (white arrow) remains near the holes, which is due to a segmentation error. Unsurprisingly, the statistical methods behave well with noisy and limited data, and the profile shows now clearly the difference of quality with the FBP-like methods. The plot of the residual error

still shows a superiority of STAT,MASK : with 20 iterations STAT,MASK has a NMSE of 0.17, compared to 0.22 for STAT, 0.28 for FBP,BHCe, 0.31 for FBP,BHCe and 0.35 for FBP.

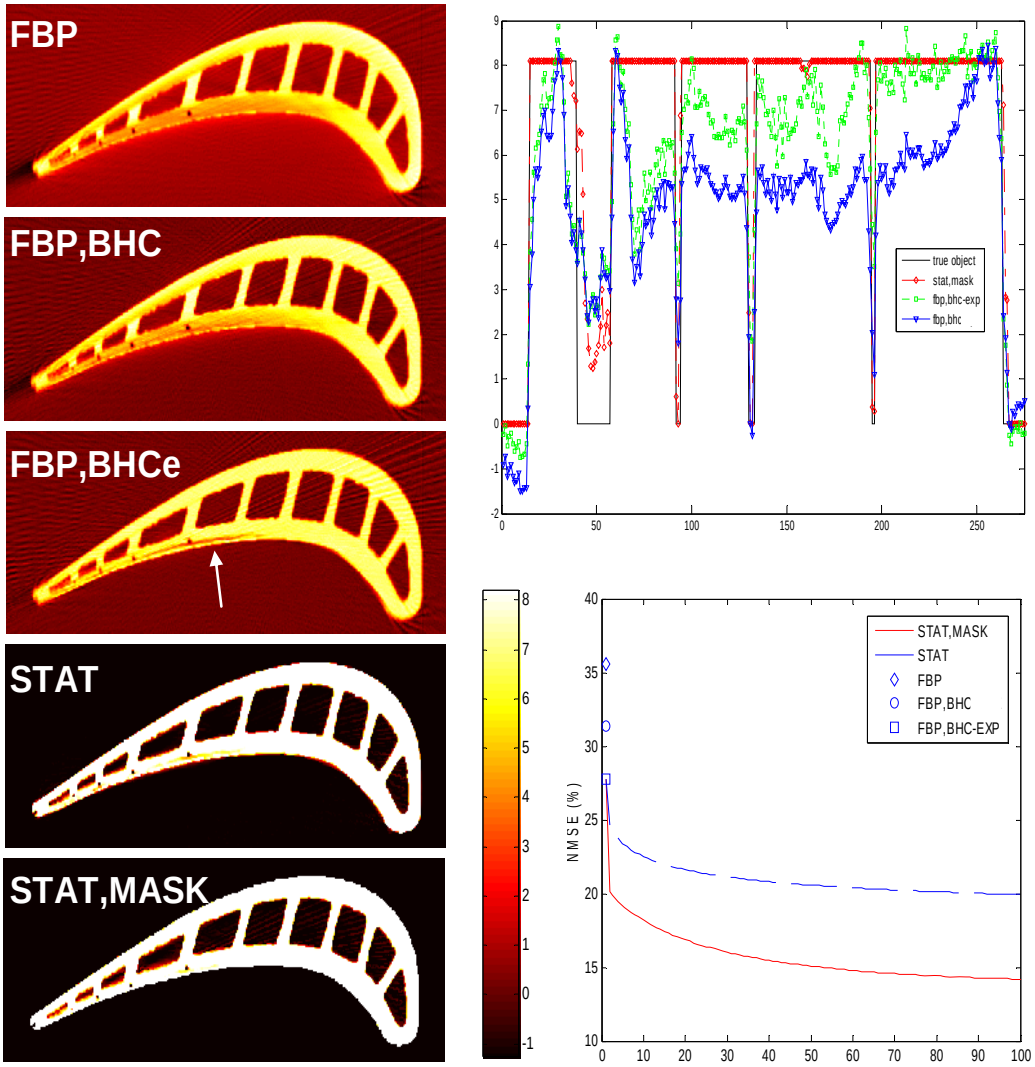

figure 6 : Reconstructed images, profile and NMSE

4 Reconstruction Results with Experimental Data

4.1 Acquisition parameters

A 2D fan beam acquisition was acquired with a 450 kV mini-focus system and a collimated linear detector with equiangular spaced pixels (figure 2). As the detector pixel spacing (2.1 mm) is large and the number of detector channels (125) is small, sub-positions are scanned to achieve a submillimetric resolution. For our experiments an acquisition mode has been used which yielded a projection data set of 720 projections and 1000 detectors, which should enable a resolution of 0.26 mm.

For the FBP,BHCe reconstruction we kept the original set of measurements (720×1000), whereas we rebinned the sinogram into a 2D fan-beam geometry with a linear detector of 601 pixels and 512 projections for the statistical method (so that STAT worked with 42 percent of the data).

4.2 Results

Fig. 7 shows the reconstructions of the FBP corrected with the experimental curve (left) and the STAT method (right). The horizontal and vertical profiles shown below, and especially along the profile B-B, exhibit a remaining beam-hardening artefact in the FBP method. A FBP-based imagery would mislead the user in its estimation of the real thickness of material in the inner part of the turbine blade. The final result shows that the statistical algorithm is able to reconstruct piecewise smooth object separated with sharp edges, with less data than standard method require, which makes it suitable for the image reconstruction in industrial CT.

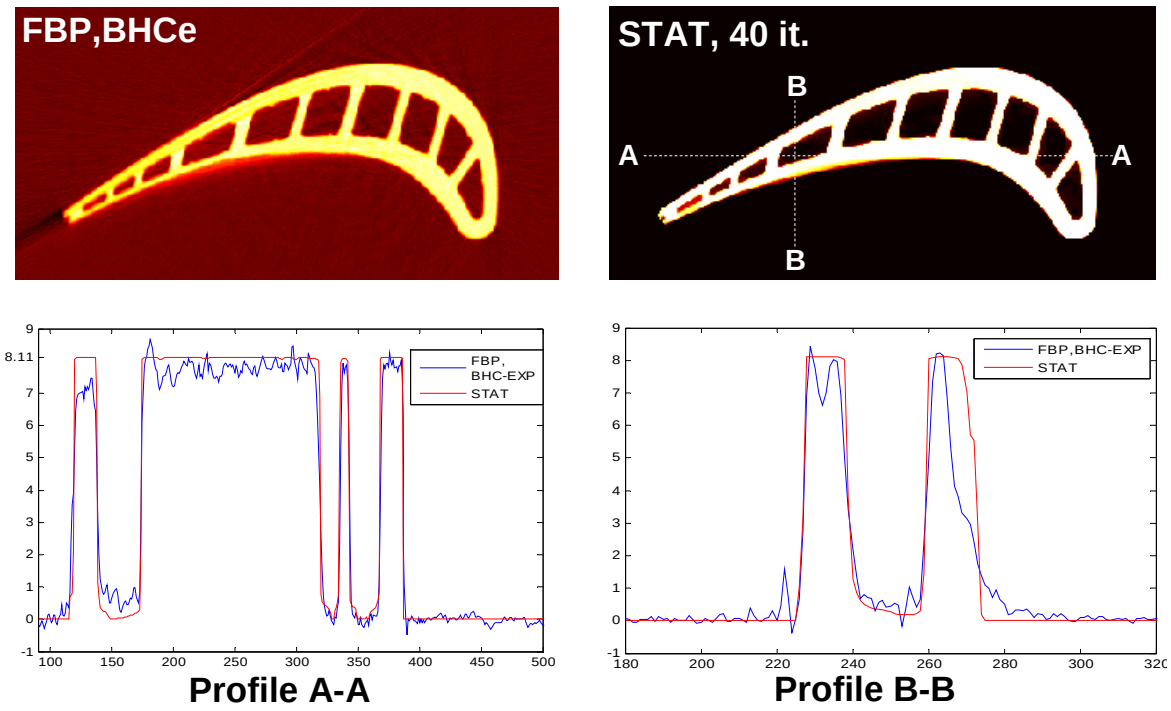

figure 7 : Reconstructed images, horizontal and vertical profiles

5. Conclusion

We used a statistical image reconstruction algorithms for polyenergetic industrial X-ray CT, and we applied it to fan beam CT scanner that is used routinely to detect flaw detection and dimensional characterization Relative to the classically available FBP method, the statistical approach significantly reduces beam hardening artefacts, and behave better in critical situations (presence of noise, limited dynamic range and reduced data). Preliminary results based on the study of the turbine blade suggest that the statistical algorithm is more accurate than FBP in quantitatively and qualitatively estimating the density.
In future work, we will investigate the impact of the scattering in uncollimated configurations. This may be important for larger objects imaged with large area detectors. An effort should be also done in the direction of the hyperparameters setting (β, δ) in order to render the algorithm more user-friendly.

Acknowledgments
The authors are grateful to the enterprise PRECICAST Ltd for the data used in section 4.2.

References

[1] Luethi T, Flisch A, Hofmann J, Obrist A, Wirth J "First article inspection based on Industrial X-ray Computed Tomography". *Topics on Non-Destructive Evaluation Series, American Society of Nondestructive Testing ASNT*, vol 6, 159-164, 2002

[2] Badel E, J-M Létang, G Peix and D Babot "Quantitative microtomography : measurement of density distribution in glass wool and local evolution during a one-dimensional compressive load", *Meas. Sci. Technol.*, vol 14 , 410-420, 2003

[3] Thierry R, Pettier J-L and Desbat L, "Simultaneous Compensation for Attenuation, Scatter and Detector Response for 2-D Emission Tomography on Nuclear Waste with Reduce Data", *1st World Conference for Industrial Process Tomography ,Buxton*, E1: 5422-5551, 1999

[4] Stampanoni M, Borchert G, and Abela R "Towards nanotomography with asymmetrically cut crystals" *Nuclear Instruments and Methods in Physics Research Section A: Accelerators, Spectrometers, Detectors and Associated Equipment*, vol 551 (1), 119-124, 2005

[5] DETECT : New Product Design and Engineering Technologies Based on Next Generation Computed Tomography. EU Project n° 203885, started date : 01.01.2004

[6] Feldkamp L.A et al "Practical Cone-Beam Algorithms" *Journal of Optical Soc. Am. A*, vol 1 (6), 612-619, 1984

[7] Krimmel S, Baumann J, Kiss Z, Kuba A,. Nagy A and.Stephan J "Discrete tomography for reconstruction from limited view angles in non-destructive testing", *Electric Notes in Discrete Math*. vol 20, 455-474, 2005

[8] Vengrinovich V, Zolotarev S. Z., Denkevich Y and Tillack G.R "New techniques for resolution enhancement in 3D X-ray tomographic imaging from incomplete data, *International symposium on CT for industrial applications and image processing in radiology*, March 15-17, Berlin 1999

[9] Nuyts J., De Man B, Dupont E, Defrise M, Suetens E and Mortelmans L "Iterative reconstruction for helical CT : A simulation study", *Phys. Med. Biol*. vol 43, 729-737, 1998

[10] De Man B, Nuyts J, Dupont P, Marchal G and Suetens P "An iterative maximum-likelihood polychromatic algorithm for CT" *IEEE Trans. Med. Imaging* 20 999–1008, 2001

[11] Elbakri I A and Fessler J A "Statistical image reconstruction for polyenergetic x-ray computed tomography" *IEEE Trans. Med. Imaging,* vol 21, 89–99, 2002

[12] Kole J.S, Beekman F.J, "Evaluation of accelerated iterative x-ray CT image reconstruction using floating point graphics hardware", *Phys. Med. Bio*, vol 51(4), 875-889, 2006

[13] Ahn A, Fessler J A, Blatt D, Hero A O, "Convergent incremental optimization transfer algorithm : application to tomography", *IEEE Trans. Med. Imaging*, vol 25(3), 283-96, 2006

[14] W. Zbijewski, F.J. Beekman, "Suppression of intensity transition artifacts in statistical X-ray computer tomography through Radon inversion initialization", *Medical Physics*, vol. 31, 62-69. 2004

[15] Joseph P M and Spital R D "A method for correcting bone induced artefacts in computed tomography scanners" *J. Comput. Assisted Tomogr*. vol 2,100–108, 1978

[16] Nalcioglu O and Lou R Y "Post-reconstruction method for beam hardening in computerized tomography" *Phys. Med. Biol.* vol 24, 330–340, 1979

[17] Alvarez R E and Macovski A "Energy-selective reconstruction in x-ray computerized tomography" *Phys. Med.Biol.*vol 21**,** 733–44, 1976

[18] Yan C H, Whalen R T, Beaupré G S, Yen S Y and Napel S "Reconstruction algorithm for polychromatic CT imaging: application to beam hardening correction" *IEEE Trans. Med. Imaging* vol 19, 1–11,2000

[19] Ruth C and Joseph P M "Estimation of a photon energy spectrum for a computed tomography scanner" *Med. Phys*. 24 695–702, 1997

[20] Hsieh J, Molthen R.C, Dawson C.A. and Johnson R.H. "An iterative approach to the beam hardening correction in cone beam CT, *Med. Phys*. 27 (1), 2000

[21] Berger M, Hubbell J, Seltzer S, Coursey J and ZuckerD1999 XCOM: photon cross sections database Technical Report National Institute of Standards and Technology (http://physics.nist.gov/PhysRefData/Xcom/Text/XCOM.html)

[22] Otsu, N., "A Threshold Selection Method from Gray-Level Histograms," *IEEE Transactions on Systems, Man, and Cybernetics*, vol. 9(1), 62-66, 1979

[23] Erdogan H and Fessler J A "Monotonic algorithms for transmission tomography" *IEEE Trans. Med. Imaging* , vol18, 801–814, 1999

[24] http://geant4.web.cern.ch/geant4/